Dynamics of magnetic phase cluster formation in the field-driven AFM–FM transition in Gd_5Ge_4

2007 J. Phys.: Condens. Matter 19 176213

(http://iopscience.iop.org/0953-8984/19/17/176213)

IOP Publishing Journal of Physics: Condensed Matter

J. Phys.: Condens. Matter **19** (2007) 176213 (7pp) doi:10.1088/0953-8984/19/17/176213

Dynamics of magnetic phase cluster formation in the field-driven AFM–FM transition in Gd_5Ge_4

G K Perkins[1], J D Moore[1], M K Chattopadhyay[2], S B Roy[2], P Chaddah[3], V K Pecharsky[3], K A Gschneidner Jr[3] and L F Cohen[1]

[1] Blackett Laboratory, Prince Consort Road, London SW7 2BZ, UK
[2] Low Temperature Physics Laboratory, Centre for Advanced Technology, Indore 452013, India
[3] Ames Laboratory and Department of Materials Science and Engineering, Iowa State University, Ames, IA 50011-3020, USA

Received 7 November 2006, in final form 19 February 2007
Published 30 March 2007
Online at stacks.iop.org/JPhysCM/19/176213

Abstract

Using a combination of local and global magnetometry, dimensional analysis and numerical simulations we investigate the dynamics of magnetic phase cluster formation across the first-order magnetic-field-driven magnetostructural transition in Gd_5Ge_4 at 6 K, where the transformation is completely irreversible, and at 35 K, where the reversibility is restored due to rising thermal fluctuations. We have previously shown, using scanning Hall probe images, that the transition involves phase separated clusters. Here we discuss these images in the context of a random nucleation and growth model, focusing on the relation between microscopic and macroscopic behaviours. The purpose of the work is to set up a framework for the analysis of these materials and it has implications for future discoveries of related functional magnetic materials where first-order, disorder-broadened transitions dominate key physical properties.

The intermetallic compound Gd_5Ge_4 [1] is a lanthanide-based naturally layered antiferromagnet (AFM) [2, 3], widely studied [4–6] in part because it is one of the parent binary compounds to a family of $Gd_5Si_{4-x}Ge_x$ giant magnetocaloric materials [7–9]. In the latter, the inherent first-order transitions between the ferromagnetic (FM) and AFM states when $x < \sim 1.2$, or between the FM and paramagnetic (PM) states when $\sim 1.7 < x < \sim 2.1$, are easily triggered by temperature, pressure [10] and/or magnetic field [11–13]. Changes in the magnetism are accompanied by martensitic-like structural transformations resulting in an unusually large isothermal magnetic entropy change, magnetostriction and magnetoresistance, and so may give rise to novel applications in magnetic refrigeration, energy conversion devices and sensors [14–16].

Magnetic imaging studies across the transition in Gd_5Ge_4 and related materials [17–19] show the process to be one of nucleation and growth, in which small FM domains initially nucleate and subsequently grow as the applied magnetic field drives the sample through the transition. Recent differential scanning calorimetry [20] and acoustic emission studies [21]

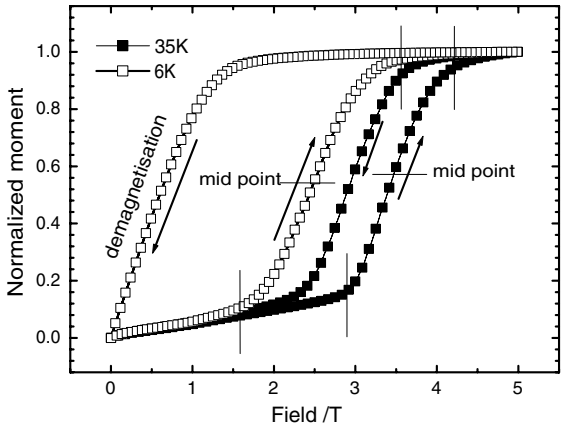

Figure 1. Normalized M–H data of the AFM–FM transition at 6 and 35 K. At 6 K, the downward cycle represents domain wall rotation of the trapped FM state, and not a transition to the AFM phase. The transition onsets and offset for the upward field cycles are indicated by vertical lines, while the midpoints are indication by horizontal lines.

point to complex kinetics of the magnetostructural transitions in many members of the $Gd_5Si_{4-x}Ge_x$ family, and indicate that they are athermal and proceed through a series of metastable states by avalanches lacking characteristic scale. Nevertheless, the relationship between the macroscopically measurable features, such as the width of the transition and the dynamics of nucleation, has not been properly established. Yet it is clearly important to understand this relationship in order to not only properly delineate processing pathways leading to improvement of the existing model compounds, but also to form a clear basic picture enabling future discoveries of novel materials with electronic, structural and magnetic properties tailored to a specific functionality, especially in response to a predetermined change of a certain thermodynamic variable.

In this paper we address the microscopic characteristics that relate to the global magnetization features and demonstrate that from direct inspection of the microscopic imaging, dimensional analysis and supporting computer simulation we can set up a form of analysis that allows us to separate the influence of nucleation from growth. We demonstrate the potential of the analysis by showing here that the difference in transition widths in Gd_5Ge_4 at two different temperatures can be related to the change in the nucleation rate and not the growth rate of the FM phase within the AFM matrix. The analysis we set up here should also have a more general significance, i.e. it is applicable to any magnetoelastic or ferroelelastic first-order phase transition.

The Gd_5Ge_4 alloy used in this study was prepared by arc-melting the mixture of pure Gd and Ge on a water-cooled copper hearth in an argon atmosphere under ambient pressure [22]. The plate-like sample with dimensions $3 \times 3 \times 0.8$ mm^3 was studied in the as-cast condition without heat treatment after it was characterized with powder x-ray diffraction and optical metallography for crystallinity and phase purity. Global magnetization was measured using a commercial vibrating sample magnetometer (Oxford Instruments 3001), while scanning Hall probe measurements were conducted using a custom-built system with a spatial resolution of $\sim$20 μm.

Figure 1 shows global magnetometry of the magnetic-field-induced AFM–FM transitions at 6 and 35 K. The M–H loops are representative of a disorder-broadened first-order phase transition, which commonly gives rise to phase separation phenomena [23]. However, at 6 K

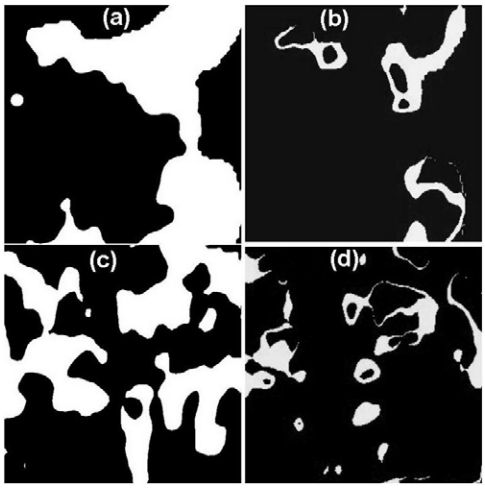

Figure 2. Scanning Hall probe images of the bulk sample midway through the AFM–FM transition. The data are represented in two-tone fashion, with black corresponding to local inductions of less than half of the saturation value while white corresponds to greater than half. At 6 K (a), the length scale of the white and dark clusters is observably larger than at 35 K (c); however, in both cases the regions are macroscopic. Images (b) (6 K) and (d) (35 K) show the difference between successive images along the $M(H)$ cycle taken at the fixed field difference of 0.1 T, highlighting the dynamics of cluster formation. All the images are 1000 μm wide.

on the downward field cycle the system is known [2, 4] to remain trapped in the FM state and the drop in magnetization results from domain rotation rather than a transition of this FM Gd_5Ge_4 phase back to the AFM state. The nature of the reversibility/irreversibility of this transition as a function of temperature has been a topic of recent studies and is not pertinent to the current discussions [9]. To avoid this complexity, the following analysis is restricted to the upward magnetic field cycle only, where the magnetic field drives the material from the AFM to the FM state at both temperatures studied. Notice from figure 1 that the onset of ferromagnetism occurs at a higher magnetic field at 35 K and the cross-over from AFM to FM (or transition width) is sharper at 35 K than at 6 K.

Direct observation of phase separation in this sample at 6 and 35 K is shown in figures 2(a) and (c). We have shown similar images previously [18, 19]. Here, scanning Hall probe imaging is used to map out the local magnetic induction on the sample surface at the midpoint of the transition (i.e. when the magnetization is half way between the saturated FM state and that of the AFM phase). For clarity, the images are shown in two-tone representation with white representing induction greater than half the FM value. The white and black regions therefore represent areas in which the FM and AFM phases dominate, respectively. Although both images represent approximately equal amounts of white and black areas, it is clear that at 6 K (figure 2(a)) the average cluster size is larger than that at 35 K (figure 2(c)), indicating quantitatively different dynamics of the underlying nucleation and growth processes. Figures 2(b) and (d) further illustrate this, showing the difference between successive fields around the onsets of the transition, i.e. 2 and 2.1 T for the 6 K isotherm, and 3.15 and 3.25 T for the 35 K isotherm. In this representation regions of growth appear as bands (sometimes fully closed to form 'doughnut' topology), where the width is directly proportional to the growth rate. Also, the number of completely filled domains (indicating new FM nucleations) is indicative of the nucleation rate. Inspection of these images suggests that for both 6 and 35 K the growth rate

of the FM domains is similar and of order 200–400 mm T^{-1}, but that at 35 K the nucleation rate is about an order of magnitude larger. Hence by experimental observation we can state that it is predominantly the nucleation rate that is responsible for the different transformation dynamics at 6 and 35 K. An increased nucleation rate at the higher temperature is clearly consistent with a thermal activation model, although in reality the physical situation is likely to be more complicated.

In order to investigate the underlying behaviour more explicitly we can apply dimensional analysis [24, 25] to the nucleation and growth scenarios, which can then be used to show how the microscopic parameters, namely the growth rate, R_G, and the nucleation rate, R_N, control the overall behaviour. It is straightforward to apply the technique to yield relations between L_C, W_T, R_G and R_N (where L_C is the characteristic cluster length scale and W_T is the transition width). In 3D, taking the dimensions of R_G as LT^{-1} and R_N as $L^{-3}T^{-1}$ indicates that L_C is proportional to $(R_G/R_N)^{0.25}$ and W_T maintains proportionality to $(R_G^3 R_N)^{-0.25}$, or that

$$R_G \propto \frac{L_C}{W_T} \tag{1}$$

$$R_N \propto \frac{1}{L_C^3 W_T}. \tag{2}$$

Relations (1) and (2) are useful because they directly relate the model parameters R_G and R_N to the experimentally accessible quantities L_C and W_T.

However, before applying dimensional relations to the experimental data we take the analysis one step further and create an artificial system to simulate the sample properties and test the dimensional analysis directly. As the simulations we perform are two-dimensional (2D), we rework the dimensional analysis accordingly. In 2D, the dimensions of R_N are $L^{-2}T^{-1}$ while those of R_G remain the same as before (i.e. LT^{-1}). We then find that the characteristic length scale should follow $L_C \propto (R_G/R_N)^{1/3}$. Hence, we expect to observe a cube root dependence of L_C on R_G/R_N in the simulations and $W_T \propto (R_G^2 R_N)^{-1/3}$

The simulation comprises a two-dimensional 500 × 500 pixel grid, where each pixel can represent either the AFM or FM state. Initially all pixels are in the AFM state and the simulation proceeds by applying successive nucleation and growth steps in the following manner. Firstly, in the nucleation step, each pixel in the grid is given a chance (determined by the nucleation rate R_N) to switch to the FM state. In the following growth step each AFM pixel that adjoins an FM pixel is given an additional chance (determined by the growth rate R_G) to switch to the FM state. Successive nucleation and growth steps are then repeated. The transition midpoint is defined when half of the pixels are in the FM state, in a similar sense to the images in figure 2. At this point the characteristic cluster size L_C, defined as the sample area divided by the total interface length between the AFM and FM states, can be calculated. The transition width W_T is determined by the number of steps required to reach the transition midpoint.

The dimensional analysis agrees surprisingly well with the simulation results shown in figures 3 and 4. Figure 3 shows that $W_T \propto R_G^{-0.7}$ from the simulation compared to the expected $W_T \propto R_G^{-0.66}$ and $W_T \propto R_{N2}^{-0.28}$ compared to the expected $W_T \propto R_N^{-0.33}$. In figure 4 (where R_G/R_N is varied by four orders of magnitude) we find $L_C \propto R_G/R_N^{0.35}$ (except where L_C approaches 1, which is the spatial resolution of the simulation) very close to the expected 1/3 power law shown by the solid line.

Having established strong support for the use of the dimensional analysis in 2D we investigate the validity of the 3D relations (1) and (2) to describe the experimental data. Figure 2 shows that at 35 K L_C is approximately half that at 6 K (we estimate 50–100 μm at 35 K and 100–200 μm at 6 K) and from global magnetometry we find $W_T \cong 1.3$ T at 35 K $W_T \cong 2$ T at 6 K (see figure 1). Therefore, relation (1) suggests that R_G is roughly

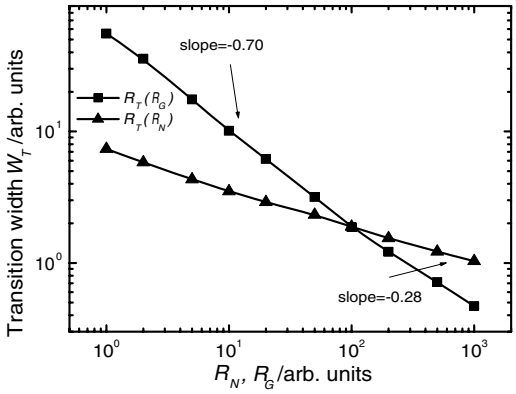

Figure 3. Simulation results showing the dependence of the transition width on both the nucleation and growth rate. The functional forms fit well to that predicted by dimensional arguments in 2D; we find $W_{\mathrm{T}} \sim R_{\mathrm{G}}^{-0.7}$ compared to the expected $W_{\mathrm{T}} \sim R_{\mathrm{G}}^{-0.66}$ and $W_{\mathrm{T}} \sim R_{\mathrm{N}}^{-0.28}$ compared to the expected $W_{\mathrm{T}} \sim R_{\mathrm{N}}^{-0.33}$.

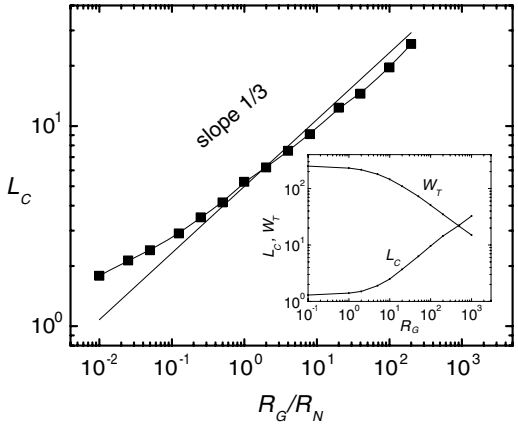

Figure 4. The variation of phase cluster length scale L_{C} with the ratio of growth rate to nucleation rate $R_{\mathrm{G}}/R_{\mathrm{N2}}$. The data from simulation (solid symbols) fit well to the cube root behaviour expected from dimensional arguments (line). Inset: the cluster length and transition width as a function of growth rate for a simulated magnetic-field-driven transition with Gaussian distribution of transition fields.

independent of temperature (at least between 6 and 35 K), while relation (2) indicates that R_{N} is around an order of magnitude greater at 35 than at 6 K. This is in good agreement with the conclusions drawn from direct inspection of the difference images in figures 2(b) and (d). A slowing down of the nucleation rate at low temperatures for example might well be consistent with observations of arrested kinetics in this system [26].

Note that the applicability of the model we have used, particularly the assumption of a constant nucleation rate, is generally unrealistic for a magnetic-field-driven transition. In this case a better description may be given by assuming a distribution of onset transition fields within the sample and then allowing the nucleation process to progress according to a simulated applied magnetic field. In this case the nucleation rate varies across the transition according to a Gaussian distribution function. For a low growth rate the transition width is given by the

width of the distribution, but if the growth rate is significant the transition will be sharper. In the inset to figure 4, we show the results of 2D simulations using a Gaussian distribution of transition onset fields. The transition width clearly saturates (roughly to that of the Gaussian) at a low growth rate (the saturation observed in L_C is an artefact of the finite pixel size). At a higher growth rate, W_T and L_C roughly follow -0.5 and $+0.5$ power dependences, respectively, rather than -0.33 and 0.66 predicted by the dimensional argument, showing a slight deviation from the predictions obtained from the dimensional analysis. However, for the purposes of this work, this discrepancy is not important and our conclusions regarding the underlying factors controlling the transition in Gd_5Ge_4 remain the same.

In summary, we have experimentally demonstrated the existence of phase cluster formation in Gd_5Ge_4. Using dimensional considerations (justified by a computer simulation) we have shown how the microscopic parameters, i.e. the growth and nucleation rates, ultimately control the observed behaviour. The experimentally measured temperature dependences of the cluster size and transition width suggest that the FM phase nucleation rate is an order of magnitude greater at 35 K than at 6 K, while the growth rate remains largely unchanged. Given that the transition width is a key to technological applications, these results may point to future strategies in the development of functional magnetic materials. In particular it is clear that it is the magnetoelastic behaviour that controls the most interesting aspects of the $Gd_5Si_{4-x}Ge_x$ giant magnetocaloric family [10, 18] as well other material systems where there is a coupled magnetic–martensitic transition such as in manganites [27]. In these systems growth rates are constrained by local volume changes during the transition and these discrete local changes are likely to be most strongly controlled by microstructure [18]. In addition the formation of clusters (of one phase embedded in the matrix of the other phase) existing on a macroscopic scale has recently been explained by the presence of long-range strain fields [28–30]. Here we show that in Gd_5Ge_4 it is the nucleation rate that changes the dynamics of the transition at the two temperatures studied. Previously it has been shown that 20 vol% of Gd_5Ge_4 is already in the FM phase when cooled to 5 K in zero field because of the addition of nucleation centres in the form of interstitial impurities [10, 11]. Hence it is clear that the nucleation rate can be increased/decreased by introducing/removing nucleation centres into/from the lattice. Many microscopic features may serve as nucleation centres (dislocations, grain boundaries, nanostructuring etc) and a complete exploration of how to engineer these materials to tailor their macroscopic properties is still lacking. Here we establish the analytical techniques that will allow for a proper description of these changes linking the microscopic parameters to the global observations.

Acknowledgments

We thank Dr A O Tsokol for preparing Gd_5Ge_4. Work at the Blackett Laboratory is supported by the Leverhulme Trust, grant number F/07 058/V. Work at Ames Laboratory is supported by the Materials Sciences Division, Office of Basic Energy Sciences of the US Department of Energy under contract no. W-7405-ENG-82 with Iowa State University of Science and Technology. The collaboration with the Centre for Advanced Materials, Indore is supported by a Royal Society international research grant.

References

[1] Szade J and Skorek G 1999 *J. Magn. Magn. Mater.* **196/197** 699
[2] Levin E M, Gschneidner K A Jr and Pecharsky V K 2002 *Phys. Rev.* B **65** 214427
[3] Magen C *et al* 2003 *J. Phys.: Condens. Matter* **15** 2389

[4] Chattopadhyay M K *et al* 2004 *Phys. Rev.* B **70** 214421
[5] Tan L *et al* 2005 *Phys. Rev.* B **71** 214408
[6] Mudryk Ya *et al* 2005 *Phys. Rev.* B **72** 064442
[7] Pecharsky V K *et al* 2003 *Phys. Rev. Lett.* **91** 197204
[8] Ugurlu O *et al* 2006 *Acta Mater.* **54** 1211
[9] Casanova F *et al* 2005 *Phys. Rev.* B **72** 172402
[10] Magen C *et al* 2003 *Phys. Rev. Lett.* **91** 207202
[11] Hardy V *et al* 2004 *Phys. Rev.* B **69** 020407
[12] Tang H *et al* 2004 *Phys. Rev.* B **69** 064410
[13] Casanova F *et al* 2004 *Phys. Rev.* B **69** 104416
[14] Pinto R P *et al* 2005 *J. Magn. Magn. Mater.* **290/291** 661
[15] Levin E M, Pecharsy V K and Gschneidner K A Jr 2001 *Phys. Rev.* B **63** 174110
[16] Nersessian N *et al* 2004 *Appl. Phys. Lett.* **84** 4801
[17] Roy S B *et al* 2004 *Phys. Rev. Lett.* **92** 147203
[18] Moore J D *et al* 2006 *Appl. Phys. Lett.* **88** 072501
[19] Moore J D *et al* 2006 *Phys. Rev.* B **73** 144426
[20] Casanova F *et al* 2004 *Eur. Phys. J.* B **40** 427
[21] Pérez-Reche F J *et al* 2006 *Phys. Rev.* B **73** 014110
[22] Pecharsky V K and Gschneider K A Jr 1997 *J. Alloys Compounds* **260** 98
[23] Imry Y and Wortis M 1979 *Phys. Rev.* B **19** 3580
[24] Buckingham E 1914 *Phys. Rev.* **4** 345
[25] Lord Rayleigh 1915 *Nature* **95** 66
[26] Roy S B *et al* 2006 *Phys. Rev.* B **74** 012403
[27] Ghivelder L and Parisi F 2005 *Phys. Rev.* B **71** 184425
[28] Moreo A, Mayr M, Feiguin A, Yunoki S and Dagotto E 2000 *Phys. Rev. Lett.* **84** 5568
[29] Burgy J, Mayr M, Martin-Mayor V, Moreo A and Dagotto E 2001 *Phys. Rev. Lett.* **87** 277202
[30] Das A K, Pampuch C, Ney A, Hasjedal T, Däweritz L, Koch R and Ploog K H 2003 *Phys. Rev. Lett.* **91** 087203